

Formation of Color Centers in Lead Iodide Perovskites: Self-Trapping and Defects in the Bulk and Surfaces

Francesco Ambrosio,* Edoardo Mosconi, Ahmed A. Alasmari, Fatmah A. S. Alasmary, Daniele Meggiolaro, and Filippo De Angelis*



Cite This: *Chem. Mater.* 2020, 32, 6916–6924



Read Online

ACCESS |



Metrics & More

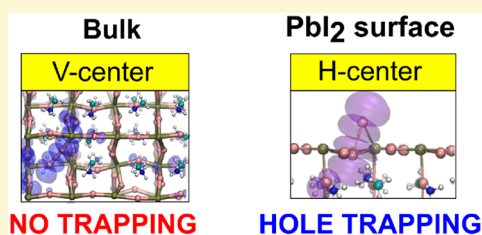


Article Recommendations



Supporting Information

ABSTRACT: Self-trapping of excitons or of free charges associated with the formation of color centers is typical of conventional halides. By analogy, lead halide perovskites could in principle show self-trapping of photogenerated charge carriers, possibly leading to defect formation and long-term material instability. Here we investigate the energetics of hole self-trapping in methylammonium lead iodide (MAPbI₃) by performing first-principles electronic structure calculations. The thermodynamics and kinetics for the formation of bridging I₂⁻ dimers and iodine vacancy/I₃⁻ trimer Frenkel defects, originated by self-trapping of one and two holes, respectively, are investigated both in the bulk and at selected surfaces, in both pristine and defective systems. Our results indicate that hole self-trapping is unlikely to occur in the bulk, being thermodynamically unfavorable with associated high-energy barriers. Self-trapping remains unfavorable at surfaces, though it is significantly stabilized compared to the bulk. The inclusion of typical hole-trapping defects, such as the lead vacancy and the interstitial iodine, further stabilizes the formation of color centers, which eventually become stable for the PbI₂-terminated MAPbI₃ surface. Overall, our results clearly indicate that surfaces and grain boundaries are the main instability sources in lead iodide perovskites and that tailoring surface passivation is crucial for improving the performance and long-term stability of devices based on lead halide perovskites.



INTRODUCTION

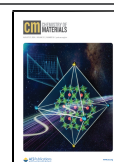
The exceptional optoelectronic properties exhibited by lead halide perovskites (LHPs) have created significant excitement for the immediate potential applications in photovoltaics but have attracted, at the same time, significant interest from a basic science point of view due to their elusive nature.^{1–4} While photoconversion efficiencies of solar cells based on optimized LHP compositions have rapidly exceeded 25%,⁵ achieving a global comprehension of the fundamental physics associated with these excellent performances has proven to be quite challenging for both experimental and theoretical models.^{6,7} In this regard, the fate and dynamics of photogenerated charge carriers remain the main issue to be investigated. In this context, the formation of spatially separated hole and electron polarons in LHPs,^{8,9} due mainly to the distortions in the soft inorganic lattice,^{10–12} has provided hints about some of the outstanding properties of LHPs,^{11–13} such as the slow bimolecular recombination coefficients,^{11–15} the low mobility of charge carriers,¹⁴ and the defect tolerance.^{15–22} Notwithstanding the recent progress, the description of some features regarding the trapping of photogenerated charge carriers remains controversial. In particular, LHPs belong to the vast family of halides for which the appearance of so-called self-trapped excitons (STEs) and the consequent formation of color centers²³ are widely documented, e.g., in alkaline and alkaline-earth halides.^{23–25}

This phenomenon, eventually leading to the trapping of electrons and holes on halide vacancies and interstitials, respectively, is traditionally described as being initiated by the formation of a metal (M)-bridging X₂⁻ dimer upon trapping of a photogenerated hole.²⁶ This defect, called a V center, involves the interaction and the displacement from their lattice sites of a neutralized halide and a X⁻.²⁶ Analogously, the interaction of an interstitial and a lattice halide leads to the formation of a so-called H center.²⁵ It is therefore tempting to explain some of the electronic properties of LHPs by invoking the occurrence of STEs, in analogy with other halides.²⁷ In particular, the formation of STEs localized on I₂⁻ dimers in MAPbI₃ (MA = methylammonium) has been proposed by electronic structure calculations.^{28,29} It was suggested that the measured high diffusion length of holes in MAPbI₃ could be associated with such self-trapped holes, on the basis of shallow trapping and of the low-energy barriers estimated for the hopping of the defect.²⁸ The formation of Pb-bridging I₂⁻ dimers was also proposed as an active mechanism of charge

Received: May 12, 2020

Revised: July 20, 2020

Published: July 21, 2020



trapping in CsPbI₃.²⁷ A possibly related self-trapping phenomenon was further proposed, which involved the formation of an iodine Frenkel defect (IFD), i.e., formation of an interstitial/vacancy I_i⁺/V_i⁺ couple, under hole-rich conditions.³⁰ The proposed mechanism involves the displacement of a lattice iodine from its position and the simultaneous formation of positively charged I vacancy and I interstitial, upon trapping of two holes.³⁰ Despite being thermodynamically feasible, this mechanism requires a very high concentration of holes,³⁰ although it is worth being considered as it may represent a perovskite degradation pathway. Moreover, the observed photoinduced degradation of MAPbI₃ has recently been explained in terms of a bimolecular reaction that involves the formation of I₂ from Pb-bridging I₂⁻ dimers and has been found to be viable only at a high concentration of I interstitials.^{15,31} While this result suggests that hole-trapping processes in bulk MAPbI₃ are mainly mediated by impurities, the possibility of self-trapping at the surface of MAPbI₃ has not yet been addressed. In this regard, it has been proposed that instability and charge loss in perovskite-based solar cells may be related to surface effects,^{32,33} the surface trap density was actually found to be ≤ 2 orders of magnitude larger than that of the bulk material, and the diffusion length of charge carriers was noticeably shorter.³⁴ Therefore, it is relevant to understand whether charge trapping at the surface of halide perovskites is unavoidable because of self-trapping or if it can be mediated only by defects (cf. refs 31 and 35), which, instead, can be reduced and passivated by chemical treatments or hindered through doping and alloying.^{31,36–45}

In this paper, we investigate through advanced electronic structure calculations the possible sources of charge self-trapping in MAPbI₃, both in the bulk and at representative surfaces. We note that self-trapping of one electron at a MAI-vacant MAPbI₃ surface was calculated to be moderately unfavorable (by 0.10 eV).³⁵ Similarly, two-electron trapping at iodine vacancies, previously envisaged through the formation of a Pb₂²⁺ dimer,⁴⁶ was found to be unstable.⁴⁷ On the basis of this background, here we focus on the thermodynamics and kinetics of hole trapping. We find that both the formation of a Pb-bridging I₂⁻ dimer and that of IDFs are implausible for the bulk phases as they are thermodynamically and kinetically impeded in pristine tetragonal and orthorhombic MAPbI₃. When considering the MAPbI₃ surface, we notice that the MAI-terminated surface, corresponding to full surface passivation, is even less supportive than the bulk material with respect to the formation of these moieties. In contrast, self-trapped holes are partly stabilized only when occurring at a PbI₂-terminated surface, representative of a fully unpassivated surface. This suggests that passivation of undercoordinated Pb sites is crucial to prevent possible endogenous degradation pathways. Furthermore, we observe that the inclusion of commonly encountered defects in MAPbI₃, such as Pb vacancies and I interstitials, aids the stabilization of hole-trapping species and lowers the energy barriers associated with their formation. We verify that MAPbI₃ degradation under hole-rich conditions, commonly associated with the ejection of molecular iodine from the surface, can occur when PbI₂ layers are (partially) exposed to the surface. Therefore, this phenomenon can be avoided by appropriate surface treatment. Our results highlight the key role of surface properties in determining the performance and long-term stability of devices based on lead halide perovskites.

METHODS

To provide an accurate representation of the electronic and trapping properties of MAPbI₃, we resort to high-level calculations at the hybrid functional level of theory. In particular, we carry out hybrid density functional theory (DFT) calculations at the PBE0+rVV10 level of theory.^{48–51} The fraction of Fock exchange α is kept fixed at its original value (0.25), as it has been found to comply with the Koopmans condition⁵² for MAPbI₃, thus ensuring that the calculations are not biased by the self-interaction error,¹¹ which would alter the energetics of the system. We include nonlocal van der Waals interactions through the rVV10 scheme, in which the b parameter governing the extent of long-range interactions is set to its original value of 6.3.^{50,51} All calculations are carried out with the freely available CP2K suite of codes.⁵³ Goedecker–Teter–Hutter pseudopotentials are used to account for core–valence interactions.⁵⁴ We use double- ζ polarized basis sets for the wave functions⁵⁵ and a cutoff of 300 Ry for the expansion of the electron density in plane waves. We employ the auxiliary density matrix method to accelerate the calculation of exact exchange in hybrid functional calculations as implemented in CP2K with the cFIT auxiliary basis set.⁵⁶ Spin-polarized calculations are performed on systems bearing an odd number of electrons.

We do not include spin–orbit coupling (SOC) in the calculations here reported. While significantly contributing to the electronic properties of lead halide perovskites^{57,58} the effect of SOC on valence band-edge states is rather limited.⁴⁷ This ensures that the properties of hole polarons, which originate from the valence band, are properly captured by our computational approach. Nevertheless, the effects of SOC on the energetics of hole-trapping species in the orthorhombic phase of MAPbI₃ have been investigated and found to be exiguous (cf. the Supporting Information for details of the calculations and of the models employed), in accord with previous studies.^{47,59}

Calculations of energy barriers are carried out using a modified version of the linear transit method⁶⁰ previously employed in ref 12. The coordinates of the structures, R_i and R_j , are linearly interpolated⁶⁰ according to the expression $R_\lambda = \lambda R_i + (1 - \lambda)R_j$, where λ is the coupling parameter connecting the two models. The initial and final models (R_i and R_j , respectively) are obtained by relaxing both MA cations and the inorganic lattice. For the R_λ structures obtained by linear interpolation of coordinates R_i and R_j , we follow a procedure ideated and tested in ref 12 to calculate energy barriers from structural configurations achieved from molecular dynamics simulations at room temperature. Because the linear interpolation of the coordinates of freely rotating cations can yield highly energetic structures, the R_λ coordinates of MA cations are relaxed while keeping fixed the intermediate R_λ coordinates of the inorganic lattice, instead of just relaxing the wave function, as in the standard linear transit method. We note that in the case of 0 K calculations, like those performed herein, the displacement of MA cations between reactants and products is exiguous, and therefore, the unmodified linear transit method is actually sufficient to produce accurate results. Indeed, by relaxing MA cations in R_λ , we achieve energy differences of < 0.01 eV with respect to the unrelaxed R_λ systems.

RESULTS AND DISCUSSION

We first consider the introduction of a single hole in tetragonal MAPbI₃. To sample the possible hole localization induced by thermal disorder, we analyze the first peak of the I–I radial distribution function [$g_{II}(r)$] obtained by 8 ps hybrid-DFT molecular dynamics simulations performed in the presence of an extra hole (cf. Figure 1a).^{11,12} A majority of the recorded I–I distances are not compatible with the formation of the I₂⁻ dimer, whose equilibrium length is 3.3 Å. The small tail in $g_{II}(r)$ appearing below 3.5 Å represents a few of the shorter distances that occur during the MD simulation. By analyzing the I–I distances for each sampled configuration, we find that I–I distances of ≤ 3.5 Å represent $\sim 5\%$ of the total configurations sampled during the MD and correspond to

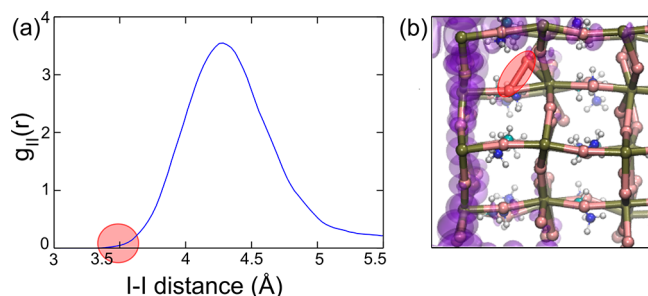


Figure 1. (a) I–I radial distribution function in tetragonal MAPbI₃ as achieved from an 8 ps molecular dynamics simulation of the system with an extra hole. (b) Isodensity representation of the hole wave function for the structural configuration featuring the shortest I–I distance (3.35 Å, highlighted with a red circle). The tetragonal axis lies horizontally.

two lattice iodines bound to the same Pb moving closer together. We then analyze the hole localization for the structural configuration in which the shortest I–I distance is recorded throughout the entire simulation. The hole is found as a polaron on a PbI₂ plane (cf. Figure 1b), in line with what is observed during the molecular dynamics,^{11,12} thus indicating that no hole localization on this transiently formed I₂[−] dimer actually takes place.

Because localization of a positive charge with formation of an I₂[−] dimer might involve an energy barrier, this could prevent us from observing this event on a picosecond time scale of *ab initio* molecular dynamics simulations, despite the occurrence of configurations with shortened I–I bonds. For this reason, we performed “static” electronic structure calculations exploring the potential energy surfaces of different models of bulk MAPbI₃ and of related surfaces (cf. the Supporting Information for the details of the considered models). For each system, we calculate the total energy differences between pristine models with an extra hole and those bearing an I₂[−] dimer (*vide infra*). We first consider the most stable structural model of tetragonal MAPbI₃, corresponding to an ordered arrangement of the MA cations.⁶¹ On this model, we perform two different calculations. (i) We inject an extra hole and relax the structure, and (ii) we move two iodine atoms at a bond length of 3.3 Å to create an I₂[−] dimer (i.e., a V center) and relax the structure with an extra hole. For the former, the hole is found to be delocalized as no hole polaron can be formed in the absence of a localizing field induced by A-site cations.¹² For the latter, upon relaxation, the dimer is retained with the hole being localized on it, with the appearance of a Kohn–Sham energy level 0.51 eV above the valence band maximum (VBM) of the material. We then consider the reaction that brings the V center from the capture of an injected hole:



$$\Delta E(V) = E(\text{I}_2^-) - E(2\text{I}^- + h^+) \quad (2)$$

where $\Delta E(V)$ is the energy of the supercell bearing a dimer and $E(2\text{I}^- + h^+)$ the energy of the pristine supercell relaxed in the presence of an extra hole. A $\Delta E(V)$ value of 0.50 eV is calculated here (cf. Figure 2a), thus indicating that dimer formation is strongly disfavored. We then employ a modified version of the linear transit method⁶⁰ (cf. Methods) to calculate the energy barrier associated with the formation of the Pb-bridging I₂[−]. The calculation evidences an energy

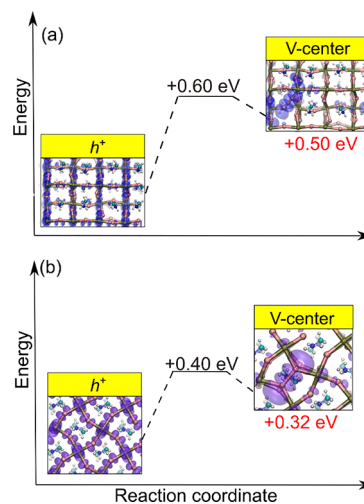


Figure 2. Schematic representation of the energetics associated with trapping of a single hole in (a) tetragonal and (b) orthorhombic MAPbI₃. Pb atoms are colored brown, I atoms pink, C atoms cyan, N atoms blue, and H atoms white. The isodensity representation of the hole is shown in purple shades for each system. The tetragonal axis lies horizontally. A closer representation is given for V centers, to aid their visualization. In each panel, the energies are referred to that of the reactant.

barrier of 0.60 eV (cf. Figure 2a) to reach the dimer structure from the starting configuration in which the hole is semilocalized, consistent with the endothermic nature of this process. Then, we consider the orthorhombic phase of MAPbI₃ (o-MAPbI₃) for which previously self-trapping of holes, through formation of an I₂[−] dimer, has been suggested.²⁸ A $\Delta E(V)$ value of 0.32 eV is calculated, thus indicating also in this case that hole self-trapping with I₂[−] dimer formation is energetically unfavorable. We note that opposite I atoms in o-MAPbI₃ (4.2 Å) are closer than in tetragonal MAPbI₃ (5.6 Å), consistent with the more favorable energetics.

Previous DFT+U calculations indicated that the I₂[−] dimer in o-MAPbI₃ is energetically favored by as much as 0.19 eV.²⁸ For this reason, we performed additional calculations employing the same computational setup of ref 28 (cf. the Supporting Information) and verified that only for extreme values of the Hubbard-like term in DFT+U calculations^{62,63} is the dimer energetically favored. In contrast, calculations of $\Delta E(V)$ including relativistic effects and an extended *k*-point sampling confirm the trend here presented (cf. the Supporting Information). At the highest level of theory employed so far on this system [$2 \times 1 \times 2$ orthorhombic supercell – 196 atoms, 1–2–1 *k*-point mesh, hybrid functional + SOC relaxation (cf. the Supporting Information)], we calculate the dimer to be 0.46 eV higher than the pristine bulk, allowing us to safely discard the spontaneous hole self-trapping with formation of an I₂[−] dimer for both kinetic and thermodynamic reasons.

As previously noticed, the presence of defects such as the lead vacancy, V_{Pb}, and the interstitial iodine, I_i, could promote the formation of I₂[−] dimers in MAPbI₃.^{15,47,64} For hole trapping at V_{Pb}, we consider the following reaction and its energetics:

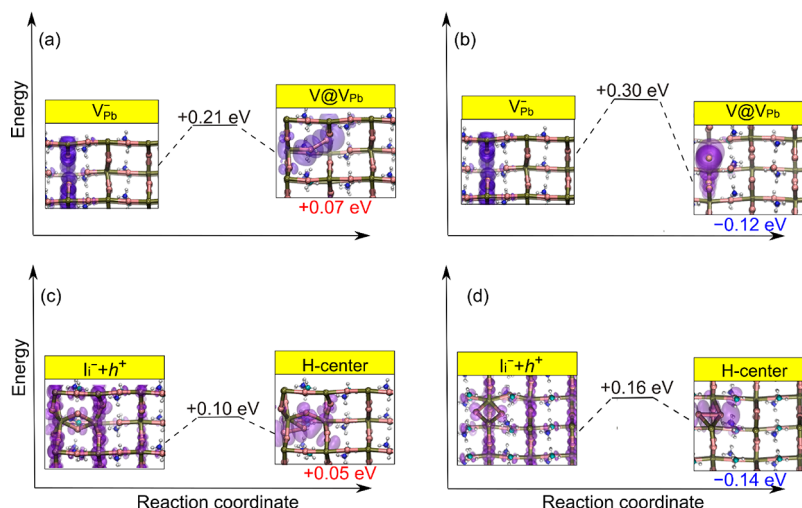
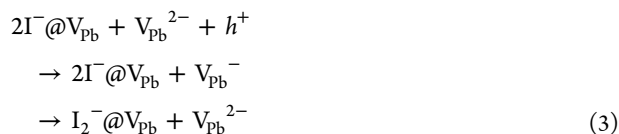


Figure 3. Schematic representation of the energetics associated with trapping of a single hole in a model of tetragonal MAPbI₃ bearing a Pb vacancy and an I interstitial. (a and c) Reaction pathways associated with the lowest energy barriers and (b and d) reaction pathways giving the most stable products. Pb atoms are colored brown, I atoms pink, C atoms cyan, N atoms blue, and H atoms white. The isodensity representation of the hole is colored purple for each system. The tetragonal axis lies horizontally. In each panel, the energies are referred to that of the reactant.



$$\begin{aligned}
 \Delta E(V@V_{\text{Pb}}) &= E(\text{I}_2^-@V_{\text{Pb}} + V_{\text{Pb}}^{2-}) \\
 &= -E(2\Gamma^-@V_{\text{Pb}} + V_{\text{Pb}}^-) \quad (4)
 \end{aligned}$$

Similarly, we can have hole trapping on a I₂⁻ dimer, through the interaction of a lattice iodine with an interstitial I, with the formation of a so-called H center:



$$\Delta E(\text{H}) = E(\text{I}_2^-) - E(\Gamma^- + \text{I}_i^- + h^+) \quad (6)$$

in which the injected hole is first semilocalized as a hole polaron and then is trapped, thus forming the I₂⁻ moiety.

We thus investigate further the energetics of hole localization at the defect site, searching for favorable energy pathways leading to the lowest barriers and most stable products, being representative of kinetically and thermodynamically preferred pathways, respectively. For hole trapping at V_{Pb}, we calculate the formation of the dimer to occur with either a lower barrier (0.21 eV) leading to a slightly unfavorable energy minimum [$\Delta E(V@V_{\text{Pb}}) = 0.07$ eV] or a higher barrier (0.30 eV) but with a more stable dimer [$\Delta E(V@V_{\text{Pb}}) = -0.12$ eV], as illustrated in panels c and d of Figure 3. Similarly, hole trapping at I_i⁻ may occur with a lower energy barrier (0.10 eV) but leading to a slightly unfavorable minimum [$\Delta E(\text{H}) = 0.05$ eV] or proceed with a slightly higher energy barrier (0.16 eV) but leading to a more stable I₂⁻ dimer [$\Delta E(\text{H}) = -0.14$ eV (cf. Figure 3c,d)]. The only difference between the two defects is that in I_i⁻ the hole is initially delocalized while a partly localized hole around the lead vacancy is observed (compare structures on the left side of panels a and b of Figure 3 and panels c and d of Figure 3). Trapping at acceptor defects is thus predicted to occur through small energy barriers in MAPbI₃, which may contribute to reduce the activity of such defects and enhance the defect tolerance of lead iodide perovskites.¹³

Considering the anticipated impact of surfaces on electron/hole localization and trapping,^{35,65} we move to the study of I₂⁻ dimers on the MAPbI₃ surface. We consider the (001) surface of tetragonal MAPbI₃, with two surface terminations, i.e., MAI-terminated and PbI₂-terminated (cf. the Supporting Information for the details and models), which are representative of a fully passivated and unpassivated surface, respectively. Injection of an extra hole results in the formation of a bulk-like and a surface-localized polaron for the MAI- and PbI₂-terminated surfaces, respectively.³⁵ For the MAI-terminated surface, a dimer can be achieved only by constraining the I–I distance during geometry optimization. Notably, we do not observe hole trapping on this constrained structure (cf. Figure 4a), and the unstable dimer structure (0.70 eV above the delocalized hole) immediately breaks if the constraint on the bond length is removed. This result is in line with the lower work function of the MAI perovskite termination impeding charge localization at states above the high-lying valence band.^{66,67} Localization of the positive charge on a Pb-bridging I₂⁻ dimer in the pristine PbI₂-terminated slab is instead only slightly energetically disfavored [$\Delta E(V) = 0.07$ eV (cf. Figure 4b)], although this process still features an appreciably high energy barrier (0.31 eV). These results highlight that unsaturated surface Pb atoms may play a major role in favoring charge trapping.

We then consider hole trapping on V_{Pb} and I_i on the PbI₂-terminated slab, because these defects have been found to be particularly stable on this surface termination.³⁵ The I₂⁻ dimer is significantly stabilized in both cases with a $\Delta E(V@V_{\text{Pb}})$ of -0.21 eV and a $\Delta E(\text{H})$ of -0.25 eV, respectively. We note that the injected hole is drawn to the terminal PbI₂ layer bearing the defect as a surface polaron for both V_{Pb} and I_i (cf. Figure 5a,b). This, in conjunction with the low energy barriers calculated [0.14 and 0.10 eV for hole trapping at V_{Pb} and I_i, respectively (cf. Figure 4)], implies a high probability of reaction and therefore of charge trapping at these surface defects. Considering the high defect density at surfaces and grain boundaries, this highlights how surface passivation is a major strategy to be pursued to further improve nonradiative deactivation of photogenerated charge carriers.

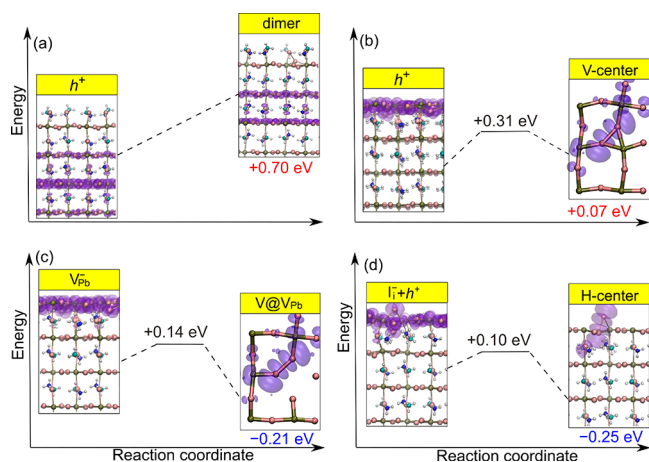


Figure 4. Schematic representation of the energetics associated with trapping of a single hole on the pristine (a) MAI-terminated and (b) PbI_2 -terminated (001) MAPbI_3 surface and on the PbI_2 -terminated system with a surface (c) a Pb vacancy and (d) an I interstitial. Pb atoms are colored brown, I atoms pink, C atoms cyan, N atoms blue, and H atoms white. The isodensity representation of the hole is colored purple for each system. A side view with the z axis of the slab lying vertically is represented in the all of the figures, with the exception of V centers in the PbI_2 -terminated slabs, for which a top view only showing Pb and I atoms is presented, to aid the visualization of the dimer. In each panel, the energies are referred to that of the reactant.

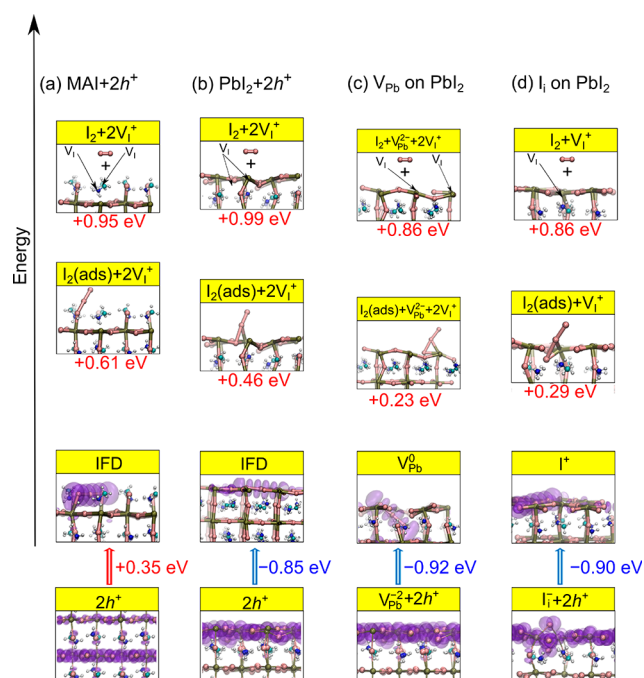


Figure 5. Schematic representation of the energetics associated with trapping of two holes in different models (pristine and defective) of the (001) surface of tetragonal MAPbI_3 . For each panel, the energy is that of the structure bearing the IFD/ I_3^- moiety. For each system, we also include the energy gain/loss associated with hole trapping on the IFD/ I_3^- moiety. Pb atoms are colored brown, I atoms pink, C atoms cyan, N atoms blue, and H atoms white. The isodensity representation of the hole is colored purple for each system. A side view with the z axis of the slab lying vertically is represented in the all of the figures. The position of surface iodine vacancies is indicated by black arrows.

We next ask what could happen by self-trapping or defect trapping of two charge holes. Despite being kinetically very unlikely, requiring the concomitant trapping of two holes at the same site, this process may become relevant under extremely hole-rich conditions. Kim et al. recently modeled the formation of an iodine vacancy/ I_3^- trimer Frenkel defect (i.e., an IFD) by the capture of two holes by the perovskite, through the following reaction:



thus involving displacement of a lattice iodide (V_1^+) and the formation of an I_3^- trimer (I_3^-).³⁰ We thus investigate the energetics of IFD formation in the MAPbI_3 bulk and at surfaces.

We define

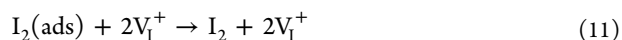
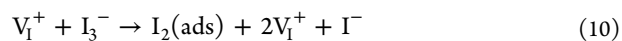
$$\begin{aligned} \Delta E(\text{IFD}) &= E(\text{V}_1^+ + \text{I}_3^-) - E(2\text{I}^- + 2\text{h}^+) \\ &= E(\text{IFD}) - E(2\text{h}^+ + 2\text{I}^-) \end{aligned} \quad (8)$$

where $E(\text{IFD})$ is the total energy of the supercell with the IFD and $E(2\text{h}^+ + 2\text{I}^-)$ the total energy of the pristine supercell with two extra holes. We note that



is found to be barrierless for both pristine and defective systems. Therefore, the energy barrier associated with the formation of an IFD is that of the capture of the first hole on the V or H center. For bulk tetragonal MAPbI_3 , we calculate a $\Delta E(\text{IFD})$ of 0.24 eV (cf. the Supporting Information). Therefore, the formation of an IFD is also energetically unfavorable in the pristine bulk perovskite, in line with the results of ref 30. IFD formation is slightly destabilized on the MAI-terminated surface [$\Delta E(\text{IFD}) = 0.35$ eV], for which the trimer is formed on the terminal MAI plane by displacement of an unsaturated I atom (cf. Figure 5a). This result is in agreement with the observed decreased stability of iodine defects on this termination.³⁵ In stark contrast, a $\Delta E(\text{IFD})$ of -0.85 eV is calculated for the PbI_2 -terminated surface (cf. Figure 5b), a result consistent with the instability of this surface associated with the lower formation energies calculated for iodine defects on the terminal PbI_2 layer.³⁵ Therefore, a high concentration of holes can indeed favor the formation of IFDs on the pristine PbI_2 -terminated surface. Notably, IFD formation can also favorably occur when a partial MAI coverage leaves the subsurface PbI_2 plane exposed. For instance, when a 50% MAI-covered slab is considered, we find a $\Delta E(\text{IFD})$ of -0.18 eV (cf. the Supporting Information). IFD formation is favored also at defect sites on the PbI_2 -terminated surface, with a stabilization comparable to that in the case of self-trapping (cf. Figure 5c,d).

Finally, we investigate the possible degradation mechanisms mediated by IFD formation at the MAPbI_3 surface under extremely hole-rich conditions. Starting from the IFD, we consider the following reaction sequence:



which ultimately leads to the loss of molecular iodine from the surface of the pristine material. Similar reactions hold when the process is mediated by a V_{Pb} and I_i . In fact, the I_3^- trimer is found as the most stable forms of V_{Pb}^0 and I_i^+ with energy levels deep in the gap of the material.^{20,35}

We calculate the total energies for each step of the reaction for both pristine surfaces and, in the PbI_2 -terminated case, in the presence of V_{Pb} and I_i . We find that reactions 10 and 11 have comparable energetics once the IFD, or equivalently the I_3^- trimer, has been formed, with I_2 release being ~ 0.9 eV higher than the corresponding IFD/I_3^- for all of the considered pristine and defective models (cf. Figure 5). The reversal of reaction 11, i.e., I_2 adsorption, is favored by 0.4–0.5 eV, in agreement with previous results.⁶⁸ The actual energetics of I_2 release is thus connected with the energy required for the formation of the IFD, which in turn is modulated by the surface work function⁶⁶ and, therefore, depends on the surface termination. As one may notice, IFD (or again I_3^- trimer) formation on PbI_2 -terminated surfaces is favored by ~ 0.9 eV for both pristine and defective slabs, thus balancing the unfavorable energetics due to I_2 release. We note that this energetics is essentially unaffected by the thickness of the employed slab model (cf. the Supporting Information). Furthermore, we note that for I_2 release as a gas-phase molecule, we have to consider an extra stabilization of ~ 0.7 eV in reaction 11, corresponding to the thermal corrections to entropy and enthalpy of gaseous I_2 .⁶⁸ Thus, while a high level of hole accumulation does not lead to perovskite degradation for MAI-terminated surfaces, the (partial) exposure of PbI_2 -terminated surfaces under extremely hole-rich conditions may lead to significant degradation of MAPbI_3 with release of gas-phase or solvated I_2 .^{51,69,70}

Overall, our analysis reveals that self-trapping of holes is undisputedly unfavorable in the bulk material, for both the tetragonal and the orthorhombic phases. In contrast, hole trapping at I_2^- dimers may be promoted by defects such as Pb vacancies and I interstitials, although for the latter a reduced hole capture probability, due to the fast hopping of the hole polaron within the material, could limit its trapping activity.^{11,12} This leaves the Pb vacancy as the main possible promoter of hole trapping in the bulk material, because the charge hole tends to be localized on the plane bearing the defect, thus implying a larger probability of hole–defect interaction. The dimer can form more easily on both the pristine and Pb-vacant PbI_2 -terminated surface of MAPbI_3 . The physical picture is almost equivalent when considering IFDs, whose formation is favored only on the PbI_2 -terminated surface of MAPbI_3 . Therefore, our results indicate that hole trapping and the possibly related degradation phenomena in MAPbI_3 are generally defect-mediated phenomena; however, PbI_2 surfaces can actually induce self-trapping of holes with the formation of IFDs even when pristine. We note, however, that photoinduced degradation can indeed occur when a very high density of defects is considered.³¹ In this context, surface treatments on MAPbI_3 have a double beneficial effect when saturating undercoordinated sites. (i) They decrease the concentration of charge traps, and (ii) they prevent surface degradation through dissociation of surface-adsorbed I_2 molecules. The reduced charge recombination measured for polycrystalline samples with excess MA cations³⁶ is consistent with the present physical picture, because MA cations passivate surface defects and unsaturated surface Pb atoms, which are ultimately responsible for charge trapping and photoinduced degradation. We note that such treatments prevent also charge trapping under electron-rich conditions. In fact, unsaturated subsurface lead atoms in MAI-vacant surfaces may actually be detached from the surface as metallic Pb under electron-rich conditions.^{35,71} Therefore, it is important to tailor the surface

perovskite properties to minimize charge loss and extend the durability of perovskite-based devices.

CONCLUSIONS

In summary, hole self-trapping in halide perovskites is demonstrated to be highly unfavorable in bulk MAPbI_3 on the basis of both thermodynamics and kinetics. Our calculations instead show that self-hole trapping is essentially a surface phenomenon, taking place at unpassivated surfaces under extremely high hole conditions. As such, this severe instability pathway, which could lead to the expulsion of I_2 from the perovskite under hole-rich regimes, can be avoided by appropriate surface treatment. By accurately quantifying the energetics of self- and defect-mediated trapping in the prototypical MAPbI_3 perovskite, we highlight the importance of properly addressing surface effects in metal halide perovskites, possibly stimulating additional dedicated experiments and surface passivation strategies.

ASSOCIATED CONTENT

Supporting Information

The Supporting Information is available free of charge at <https://pubs.acs.org/doi/10.1021/acs.chemmater.0c02005>.

A detailed description of the models employed, an analysis of the impact of the thickness of the slab on the electronic properties of IFDs, $\Delta E(\text{V})$ for o- MAPbI_3 at various levels of theory, list of $\Delta E(\text{IFD})$ values for different systems, representation of hole trapping in bulk tetragonal MAPbI_3 and on the 50% MAI-covered (001) surface, and additional references (PDF)

AUTHOR INFORMATION

Corresponding Authors

Francesco Ambrosio – *CompuNet, Istituto Italiano di Tecnologia, 16163 Genova, Italy; Computational Laboratory for Hybrid/Organic Photovoltaics (CLHYO), Istituto CNR di Scienze e Tecnologie Chimiche “Giulio Natta” (CNR-SCITEC), 06123 Perugia, Italy; orcid.org/0000-0002-6388-9586; Email: Francesco.Ambrosio@iit.it*

Filippo De Angelis – *CompuNet, Istituto Italiano di Tecnologia, 16163 Genova, Italy; Computational Laboratory for Hybrid/Organic Photovoltaics (CLHYO), Istituto CNR di Scienze e Tecnologie Chimiche “Giulio Natta” (CNR-SCITEC), 06123 Perugia, Italy; Chemistry Department, College of Science, King Saud University, Riyadh 12372, Saudi Arabia; Department of Chemistry, Biology and Biotechnology, University of Perugia, 06123 Perugia, Italy; orcid.org/0000-0003-3833-1975; Email: filippo@thch.unipg.it*

Authors

Edoardo Mosconi – *Computational Laboratory for Hybrid/Organic Photovoltaics (CLHYO), Istituto CNR di Scienze e Tecnologie Chimiche “Giulio Natta” (CNR-SCITEC), 06123 Perugia, Italy; orcid.org/0000-0001-5075-6664*

Ahmed A. Alasmari – *The First Industrial Institute, TVTC, Riyadh 12613, Saudi Arabia; Physics and Astronomy Department, College of Science, King Saud University, Riyadh 12372, Saudi Arabia*

Fatmah A. S. Alasmary – *Chemistry Department, College of Science, King Saud University, Riyadh 12372, Saudi Arabia*

Daniele Meggiolaro – *Computational Laboratory for Hybrid/Organic Photovoltaics (CLHYO), Istituto CNR di Scienze e*

Tecnologie Chimiche "Giulio Natta" (CNR-SCITEC), 06123 Perugia, Italy; orcid.org/0000-0001-9717-133X

Complete contact information is available at:
<https://pubs.acs.org/10.1021/acs.chemmater.0c02005>

Notes

The authors declare no competing financial interest.

ACKNOWLEDGMENTS

This work was supported by the Distinguished Scientist Fellowship Program (DSFP) of King Saud University. E.M. has received funding from the European Union's Horizon 2020 research and innovation programme under Grant Agreement 764047 of the ESPRESSO project. The Ministero dell'Istruzione dell'Università e della Ricerca (MIUR) and Università degli Studi di Perugia are acknowledged for financial support through the program "Dipartimenti di Eccellenza 2018-2022" (Grant AMIS) to F.D.A.

REFERENCES

- (1) Etgar, L.; Gao, P.; Xue, Z.; Peng, Q.; Chandiran, A. K.; Liu, B.; Nazeeruddin, M. K.; Grätzel, M. Mesoscopic $\text{CH}_3\text{NH}_3\text{PbI}_3/\text{TiO}_2$ Heterojunction Solar Cells. *J. Am. Chem. Soc.* **2012**, *134* (42), 17396–17399.
- (2) Burschka, J.; Pellet, N.; Moon, S.-J.; Humphry-Baker, R.; Gao, P.; Nazeeruddin, M. K.; Grätzel, M. Sequential Deposition as a Route to High-Performance Perovskite-Sensitized Solar Cells. *Nature* **2013**, *499*, 316.
- (3) Brenner, T. M.; Egger, D. A.; Kronik, L.; Hodes, G.; Cahen, D. Hybrid Organic–Inorganic Perovskites: Low-Cost Semiconductors with Intriguing Charge-Transport Properties. *Nat. Rev. Mater.* **2016**, *1*, 15007.
- (4) Meggiolaro, D.; Ambrosio, F.; Mosconi, E.; Mahata, A.; De Angelis, F. Polarons in Metal Halide Perovskites. *Adv. Energy Mater.* **2020**, *10*, 1902748.
- (5) National Renewable Energy Laboratory (NREL) website. <https://www.nrel.gov/pv/assets/images/efficiency-chart.png> (accessed 2019-09-13).
- (6) Filippetti, A.; Delugas, P.; Mattoni, A. Radiative Recombination and Photoconversion of Methylammonium Lead Iodide Perovskite by First Principles: Properties of an Inorganic Semiconductor within a Hybrid Body. *J. Phys. Chem. C* **2014**, *118* (43), 24843–24853.
- (7) Sell, D. D.; Casey, H. C. Optical Absorption and Photoluminescence Studies of Thin GaAs Layers in $\text{GaAs}-\text{Al}_x\text{Ga}_{1-x}\text{As}$ Double Heterostructures. *J. Appl. Phys.* **1974**, *45* (2), 800–807.
- (8) Miyata, K.; Meggiolaro, D.; Trinh, M. T.; Joshi, P. P.; Mosconi, E.; Jones, S. C.; De Angelis, F.; Zhu, X. Y. Large Polarons in Lead Halide Perovskites. *Sci. Adv.* **2017**, *3* (8), No. e1701217.
- (9) Cinquanta, E.; Meggiolaro, D.; Motti, S. G.; Gandini, M.; Alcocer, M. J. P.; Akkerman, Q. A.; Vozzi, C.; Manna, L.; De Angelis, F.; Petrozza, A.; Stagira, S. Ultrafast THz Probe of Photoinduced Polarons in Lead-Halide Perovskites. *Phys. Rev. Lett.* **2019**, *122* (16), 166601.
- (10) Yaffe, O.; Guo, Y.; Tan, L. Z.; Egger, D. A.; Hull, T.; Stoumpos, C. C.; Zheng, F.; Heinz, T. F.; Kronik, L.; Kanatzidis, M. G.; Owen, J. S.; Rappe, A. M.; Pimenta, M. A.; Brus, L. E. Local Polar Fluctuations in Lead Halide Perovskite Crystals. *Phys. Rev. Lett.* **2017**, *118* (13), 136001.
- (11) Ambrosio, F.; Wiktor, J.; De Angelis, F.; Pasquarello, A. Origin of Low Electron–Hole Recombination Rate in Metal Halide Perovskites. *Energy Environ. Sci.* **2018**, *11* (1), 101–105.
- (12) Ambrosio, F.; Meggiolaro, D.; Mosconi, E.; De Angelis, F. Charge Localization, Stabilization, and Hopping in Lead Halide Perovskites: Competition between Polaron Stabilization and Cation Disorder. *ACS Energy Lett.* **2019**, *4* (8), 2013–2020.
- (13) Wiktor, J.; Ambrosio, F.; Pasquarello, A. Mechanism Suppressing Charge Recombination at Iodine Defects in $\text{CH}_3\text{NH}_3\text{PbI}_3$ by Polaron Formation. *J. Mater. Chem. A* **2018**, *6* (35), 16863–16867.
- (14) Brenner, T. M.; Egger, D. A.; Rappe, A. M.; Kronik, L.; Hodes, G.; Cahen, D. Are Mobilities in Hybrid Organic–Inorganic Halide Perovskites Actually “High”? *J. Phys. Chem. Lett.* **2015**, *6* (23), 4754–4757.
- (15) Motti, S. G.; Meggiolaro, D.; Martani, S.; Sorrentino, R.; Barker, A. J.; De Angelis, F.; Petrozza, A. Defect Activity in Metal–Halide Perovskites. *Adv. Mater.* **2019**, *31*, 1901183.
- (16) Kim, J.; Lee, S.-H.; Lee, J. H.; Hong, K.-H. The Role of Intrinsic Defects in Methylammonium Lead Iodide Perovskite. *J. Phys. Chem. Lett.* **2014**, *5* (8), 1312–1317.
- (17) Yamada, Y.; Endo, M.; Wakamiya, A.; Kanemitsu, Y. Spontaneous Defect Annihilation in $\text{CH}_3\text{NH}_3\text{PbI}_3$ Thin Films at Room Temperature Revealed by Time-Resolved Photoluminescence Spectroscopy. *J. Phys. Chem. Lett.* **2015**, *6* (3), 482–486.
- (18) Buin, A.; Pietsch, P.; Xu, J.; Voznyy, O.; Ip, A. H.; Comin, R.; Sargent, E. H. Materials Processing Routes to Trap-Free Halide Perovskites. *Nano Lett.* **2014**, *14* (11), 6281–6286.
- (19) Dagnall, K. A.; Foley, B. J.; Cuthriell, S. A.; Alpert, M. R.; Deng, X.; Chen, A. Z.; Sun, Z.; Gupta, M. C.; Xiao, K.; Lee, S.-H.; Ma, Y.-Z.; Choi, J. J. Relationship between the Nature of Monovalent Cations and Charge Recombination in Metal Halide Perovskites. *ACS Appl. Energy Mater.* **2020**, *3*, 1298.
- (20) Meggiolaro, D.; Motti, S. G.; Mosconi, E.; Barker, A. J.; Ball, J.; Andrea Riccardo Perini, C.; Deschler, F.; Petrozza, A.; De Angelis, F. Iodine Chemistry Determines the Defect Tolerance of Lead-Halide Perovskites. *Energy Environ. Sci.* **2018**, *11* (3), 702–713.
- (21) Chu, W.; Zheng, Q.; Prezhdo, O. V.; Zhao, J.; Saidi, W. A. Low-Frequency Lattice Phonons in Halide Perovskites Explain High Defect Tolerance Toward Electron–Hole Recombination. *Sci. Adv.* **2020**, *6* (7), eaaw7453.
- (22) Chu, W.; Saidi, W. A.; Zhao, J.; Prezhdo, O. V. Soft Lattice and Defect Covalency Rationalize Tolerance of $\beta\text{-CsPbI}_3$ Perovskite Solar Cells to Native Defects. *Angew. Chem., Int. Ed.* **2020**, *59* (16), 6435–6441.
- (23) Stoneham, A. M. *Theory of defects in solids: electronic structure of defects in insulators and semiconductors*; Clarendon Press: Oxford, U.K., 2001.
- (24) Sonder, E.; Sibley, W. A. *Point defects in solids*; Plenum Press: New York, 1972.
- (25) Williams, R. T.; Song, K. S. The Self-Trapped Exciton. *J. Phys. Chem. Solids* **1990**, *51* (7), 679–716.
- (26) Popov, A. I.; Kotomin, E. A.; Maier, J. Analysis of Self-Trapped Hole Mobility in Alkali Halides and Metal Halides. *Solid State Ionics* **2017**, *302*, 3–6.
- (27) Evarestov, R. A.; Senocrate, A.; Kotomin, E. A.; Maier, J. First-Principles Calculations of Iodine-Related Point Defects in CsPbI_3 . *Phys. Chem. Chem. Phys.* **2019**, *21* (15), 7841–7846.
- (28) Peng, C.; Wang, J.; Wang, H.; Hu, P. Unique Trapped Dimer State of the Photogenerated Hole in Hybrid Orthorhombic $\text{CH}_3\text{NH}_3\text{PbI}_3$ Perovskite: Identification, Origin, and Implications. *Nano Lett.* **2017**, *17* (12), 7724–7730.
- (29) Whalley, L. D.; Crespo-Otero, R.; Walsh, A. H-Center and V-Center Defects in Hybrid Halide Perovskites. *ACS Energy Lett.* **2017**, *2* (12), 2713–2714.
- (30) Kim, S. H.; Lee, D. Role of Charge-Trapping Iodine Frenkel Defects for Hysteresis in Organic–Inorganic Hybrid Perovskite from First-Principles Calculations. *J. Phys. Chem. C* **2019**, *123* (14), 9629–9633.
- (31) Motti, S. G.; Meggiolaro, D.; Barker, A. J.; Mosconi, E.; Perini, C. A. R.; Ball, J. M.; Gandini, M.; Kim, M.; De Angelis, F.; Petrozza, A. Controlling Competing Photochemical Reactions Stabilizes Perovskite Solar Cells. *Nat. Photonics* **2019**, *13* (8), 532–539.
- (32) Schulz, P.; Cahen, D.; Kahn, A. Halide Perovskites: Is It All about the Interfaces? *Chem. Rev.* **2019**, *119* (5), 3349–3417.

- (33) Ono, L. K.; Qi, Y. Surface and Interface Aspects of Organometal Halide Perovskite Materials and Solar Cells. *J. Phys. Chem. Lett.* **2016**, *7* (22), 4764–4794.
- (34) Wu, B.; Nguyen, H. T.; Ku, Z.; Han, G.; Giovanni, D.; Mathews, N.; Fan, H. J.; Sum, T. C. Discerning the Surface and Bulk Recombination Kinetics of Organic–Inorganic Halide Perovskite Single Crystals. *Adv. Energy Mater.* **2016**, *6* (14), 1600551.
- (35) Ambrosio, F.; Meggiolaro, D.; Mosconi, E.; De Angelis, F. Charge Localization and Tapping at Surfaces in Lead-Iodide Perovskites: The Role of Polarons and Defects. *J. Mater. Chem. A* **2020**, *8* (14), 6882–6892.
- (36) Yang, Y.; Yang, M.; Moore, D. T.; Yan, Y.; Miller, E. M.; Zhu, K.; Beard, M. C. Top and Bottom Surfaces Limit Carrier Lifetime in Lead Iodide Perovskite Films. *Nat. Energy* **2017**, *2*, 16207.
- (37) Xu, J.; Buin, A.; Ip, A. H.; Li, W.; Voznyy, O.; Comin, R.; Yuan, M.; Jeon, S.; Ning, Z.; McDowell, J. J.; Kanjanaboos, P.; Sun, J.-P.; Lan, X.; Quan, L. N.; Kim, D. H.; Hill, I. G.; Maksymovych, P.; Sargent, E. H. Perovskite–Fullerene Hybrid Materials Suppress Hysteresis in Planar Diodes. *Nat. Commun.* **2015**, *6*, 7081.
- (38) Zhang, H.; Wu, Y.; Shen, C.; Li, E.; Yan, C.; Zhang, W.; Tian, H.; Han, L.; Zhu, W.-H. Efficient and Stable Chemical Passivation on Perovskite Surface via Bidentate Anchoring. *Adv. Energy Mater.* **2019**, *9* (13), 1803573.
- (39) Noel, N. K.; Abate, A.; Stranks, S. D.; Parrott, E. S.; Burlakov, V. M.; Goriely, A.; Snaith, H. J. Enhanced Photoluminescence and Solar Cell Performance via Lewis Base Passivation of Organic–Inorganic Lead Halide Perovskites. *ACS Nano* **2014**, *8* (10), 9815–9821.
- (40) Yang, S.; Dai, J.; Yu, Z.; Shao, Y.; Zhou, Y.; Xiao, X.; Zeng, X. C.; Huang, J. Tailoring Passivation Molecular Structures for Extremely Small Open-Circuit Voltage Loss in Perovskite Solar Cells. *J. Am. Chem. Soc.* **2019**, *141* (14), 5781–5787.
- (41) Wang, Q.; Mosconi, E.; Wolff, C.; Li, J.; Neher, D.; De Angelis, F.; Suranna, G. P.; Grisorio, R.; Abate, A. Rationalizing the Molecular Design of Hole-Selective Contacts to Improve Charge Extraction in Perovskite Solar Cells. *Adv. Energy Mater.* **2019**, *9* (28), 1900990.
- (42) Ju, D.; Dang, Y.; Zhu, Z.; Liu, H.; Chueh, C.-C.; Li, X.; Wang, L.; Hu, X.; Jen, A. K. Y.; Tao, X. Tunable Band Gap and Long Carrier Recombination Lifetime of Stable Mixed $\text{CH}_3\text{NH}_3\text{Pb}_{1-x}\text{Sn}_x\text{I}_3$ Single Crystals. *Chem. Mater.* **2018**, *30* (5), 1556–1565.
- (43) Pisanu, A.; Mahata, A.; Mosconi, E.; Patrini, M.; Quadrelli, P.; Milanese, C.; De Angelis, F.; Malavasi, L. Exploring the Limits of Three-Dimensional Perovskites: The Case of $\text{FAPb}_{1-x}\text{Sn}_x\text{Br}_3$. *ACS Energy Lett.* **2018**, *3* (6), 1353–1359.
- (44) Eperon, G. E.; Leijtens, T.; Bush, K. A.; Prasanna, R.; Green, T.; Wang, J. T.-W.; McMeeekin, D. P.; Volonakis, G.; Milot, R. L.; May, R.; Palmstrom, A.; Slotcavage, D. J.; Belisle, R. A.; Patel, J. B.; Parrott, E. S.; Sutton, R. J.; Ma, W.; Moghadam, F.; Conings, B.; Babayigit, A.; Boyen, H.-G.; Bent, S.; Giustino, F.; Herz, L. M.; Johnston, M. B.; McGehee, M. D.; Snaith, H. J. Perovskite-Perovskite Tandem Photovoltaics with Optimized Band Gaps. *Science* **2016**, *354* (6314), 861.
- (45) Yang, Z.; Rajagopal, A.; Chueh, C.-C.; Jo, S. B.; Liu, B.; Zhao, T.; Jen, A. K. Y. Stable Low-Bandgap Pb–Sn Binary Perovskites for Tandem Solar Cells. *Adv. Mater.* **2016**, *28* (40), 8990–8997.
- (46) Agiorgousis, M. L.; Sun, Y.-Y.; Zeng, H.; Zhang, S. Strong Covalency-Induced Recombination Centers in Perovskite Solar Cell Material $\text{CH}_3\text{NH}_3\text{PbI}_3$. *J. Am. Chem. Soc.* **2014**, *136* (41), 14570–14575.
- (47) Meggiolaro, D.; De Angelis, F. First-Principles Modeling of Defects in Lead Halide Perovskites: Best Practices and Open Issues. *ACS Energy Lett.* **2018**, *3* (9), 2206–2222.
- (48) Perdew, J. P.; Ernzerhof, M.; Burke, K. Rationale for Mixing Exact Exchange with Density Functional Approximations. *J. Chem. Phys.* **1996**, *105* (22), 9982–9985.
- (49) Adamo, C.; Barone, V. Toward Reliable Density Functional Methods without Adjustable Parameters: The PBE0 Model. *J. Chem. Phys.* **1999**, *110* (13), 6158–6170.
- (50) Vydrov, O. A.; Van Voorhis, T. Nonlocal van der Waals Density Functional: The Simpler the Better. *J. Chem. Phys.* **2010**, *133* (24), 244103.
- (51) Sabatini, R.; Gorni, T.; De Gironcoli, S. Nonlocal van der Waals Density Functional Made Simple and Efficient. *Phys. Rev. B: Condens. Matter Mater. Phys.* **2013**, *87* (4), No. 041108.
- (52) Perdew, J. P.; Parr, R. G.; Levy, M.; Balduz, J. L. Density-Functional Theory for Fractional Particle Number: Derivative Discontinuities of the Energy. *Phys. Rev. Lett.* **1982**, *49* (23), 1691–1694.
- (53) VandeVondele, J.; Krack, M.; Mohamed, F.; Parrinello, M.; Chassaing, T.; Hutter, J. Quickstep: Fast and Accurate Density Functional Calculations Using a Mixed Gaussian and Plane Waves Approach. *Comput. Phys. Commun.* **2005**, *167* (2), 103–128.
- (54) Goedecker, S.; Teter, M.; Hutter, J. Separable Dual-Space Gaussian Pseudopotentials. *Phys. Rev. B: Condens. Matter Mater. Phys.* **1996**, *54* (3), 1703.
- (55) VandeVondele, J.; Hutter, J. Gaussian Basis Sets for Accurate Calculations on Molecular Systems in Gas and Condensed Phases. *J. Chem. Phys.* **2007**, *127* (11), 114105.
- (56) Guidon, M.; Hutter, J.; VandeVondele, J. Auxiliary Density Matrix Methods for Hartree–Fock Exchange Calculations. *J. Chem. Theory Comput.* **2010**, *6* (8), 2348–2364.
- (57) Even, J.; Pedesseau, L.; Jancu, J.-M.; Katan, C. Importance of Spin–Orbit Coupling in Hybrid Organic/Inorganic Perovskites for Photovoltaic Applications. *J. Phys. Chem. Lett.* **2013**, *4* (17), 2999–3005.
- (58) Umari, P.; Mosconi, E.; De Angelis, F. Relativistic GW Calculations on $\text{CH}_3\text{NH}_3\text{PbI}_3$ and $\text{CH}_3\text{NH}_3\text{SnI}_3$ Perovskites for Solar Cell Applications. *Sci. Rep.* **2015**, *4*, 4467.
- (59) Hao, F.; Stoumpos, C. C.; Chang, R. P. H.; Kanatzidis, M. G. Anomalous Band Gap Behavior in Mixed Sn and Pb Perovskites Enables Broadening of Absorption Spectrum in Solar Cells. *J. Am. Chem. Soc.* **2014**, *136* (22), 8094–8099.
- (60) Halgren, T. A.; Lipscomb, W. N. The Synchronous-Transit Method for Determining Reaction Pathways and Locating Molecular Transition States. *Chem. Phys. Lett.* **1977**, *49* (2), 225–232.
- (61) Quarti, C.; Mosconi, E.; De Angelis, F. Interplay of Orientational Order and Electronic Structure in Methylammonium Lead Iodide: Implications for Solar Cell Operation. *Chem. Mater.* **2014**, *26* (22), 6557–6569.
- (62) Liechtenstein, A. I.; Anisimov, V. I.; Zaanen, J. Density-Functional Theory and Strong Interactions: Orbital Ordering in Mott–Hubbard Insulators. *Phys. Rev. B: Condens. Matter Mater. Phys.* **1995**, *52* (8), R5467–R5470.
- (63) Dudarev, S. L.; Botton, G. A.; Savrasov, S. Y.; Humphreys, C. J.; Sutton, A. P. Electron-Energy-Loss Spectra and the Structural Stability of Nickel Oxide: An LSDA+U study. *Phys. Rev. B: Condens. Matter Mater. Phys.* **1998**, *57* (3), 1505–1509.
- (64) Du, M.-H. Density Functional Calculations of Native Defects in $\text{CH}_3\text{NH}_3\text{PbI}_3$: Effects of Spin–Orbit Coupling and Self-Interaction Error. *J. Phys. Chem. Lett.* **2015**, *6* (8), 1461–1466.
- (65) Meggiolaro, D.; Mosconi, E.; De Angelis, F. Formation of Surface Defects Dominates Ion Migration in Lead-Halide Perovskites. *ACS Energy Lett.* **2019**, *4* (3), 779–785.
- (66) Meggiolaro, D.; Mosconi, E.; Proppe, A. H.; Quintero-Bermudez, R.; Kelley, S. O.; Sargent, E. H.; De Angelis, F. Energy Level Tuning at the MAPbI_3 Perovskite/Contact Interface Using Chemical Treatment. *ACS Energy Lett.* **2019**, *4* (9), 2181–2184.
- (67) Quarti, C.; De Angelis, F.; Beljonne, D. Influence of Surface Termination on the Energy Level Alignment at the $\text{CH}_3\text{NH}_3\text{PbI}_3$ Perovskite/ C_{60} Interface. *Chem. Mater.* **2017**, *29* (3), 958–968.
- (68) Meggiolaro, D.; Mosconi, E.; De Angelis, F. Modeling the Interaction of Molecular Iodine with MAPbI_3 : A Probe of Lead-Halide Perovskites Defect Chemistry. *ACS Energy Lett.* **2018**, *3* (2), 447–451.
- (69) Kim, G. Y.; Senocrate, A.; Yang, T.-Y.; Gregori, G.; Grätzel, M.; Maier, J. Large Tunable Photoeffect on Ion Conduction in Halide

Perovskites and Implications for Photodecomposition. *Nat. Mater.* **2018**, *17* (5), 445–449.

(70) Samu, G. F.; Balog, Á.; De Angelis, F.; Meggiolaro, D.; Kamat, P. V.; Janáky, C. Electrochemical Hole Injection Selectively Expels Iodide from Mixed Halide Perovskite Films. *J. Am. Chem. Soc.* **2019**, *141* (27), 10812–10820.

(71) Sadoughi, G.; Starr, D. E.; Handick, E.; Stranks, S. D.; Gorgoi, M.; Wilks, R. G.; Bär, M.; Snaith, H. J. Observation and Mediation of the Presence of Metallic Lead in Organic–Inorganic Perovskite Films. *ACS Appl. Mater. Interfaces* **2015**, *7* (24), 13440–13444.